Optics Letters

Slit-enabled linear-array photoacoustic tomography with near isotropic spatial resolution in three dimensions

YUEHANG WANG, DEPENG WANG, YUMIAO ZHANG, JUMIN GENG, JONATHAN F. LOVELL, AND JUN XIA*

Department of Biomedical Engineering, University at Buffalo, State University of New York, Buffalo, New York 14260, USA
**Corresponding author: junxia@buffalo.edu*

Received 25 September 2015; revised 10 November 2015; accepted 23 November 2015; posted 24 November 2015 (Doc. ID 250696); published 21 December 2015

Due to its unique capability of visualizing optical absorption in deep tissues, photoacoustic tomography is increasingly used in biomedical imaging. Among various types of transducer arrays, the linear array is perhaps the most widely used in photoacoustic tomography because it is commercially available and readily allows ultrasound imaging. However, the three-dimensional imaging capability of a linear array is limited due to its poor elevational resolution. While various scanning schemes have been proposed to address this problem, they all suffer from long scanning time to the best of our knowledge. To address this issue, we introduce slit-enabled three-dimensional photoacoustic tomography. The metal slit, placed at the array focus, causes the incoming photoacoustic waves to diffract along the elevation direction and, hence, significantly improves the elevation detection aperture and resolution. We tested the new system in both phantoms and animals. The slit improves the elevation resolution by 10 times without compromising scanning time.

OCIS codes: (050.1940) Diffraction; (110.5120) Photoacoustic imaging; (110.5125) Photoacoustics; (110.7170) Ultrasound; (110.6960) Tomography.

http://dx.doi.org/10.1364/OL.41.000127

Photoacoustic (PA) tomography (PAT) is playing an increasingly important role in biomedical imaging. The hybrid nature of PAT allows acquisition of high-resolution images beyond the optical diffusion limit [1–4]. Among various transducer arrays used in PAT, linear transducer arrays are commonly seen due to their low cost, hand-held convenience, and easy adaption to clinical applications [5–8]. However, the three-dimensional (3D) imaging capability of a linear array is limited because its elevation resolution is much worse than the axial and lateral spatial resolutions. For instance, a Philips L7-4 array has a 0.144 mm axial and 0.298 mm lateral resolutions, but only a 1.5 mm elevation resolution (at the acoustic focus). Over the past few years, multiple methods have been proposed to address this issue. Gateau *et al.* combined linear and rotational scanning to achieve nearly isotropic 3D spatial resolution [9]. Schwarz *et al.* proposed a bi-directional scan method with two array positions perpendicular to each other [10]. In principle, all these methods improve elevation resolution by converting the elevation direction into axial or lateral directions. However, such complicated scanning geometry often requires prolonged scanning times.

In this Letter, we propose a fundamentally different approach to improve elevation resolution. Our method is based on acoustic diffraction through a thin slit placed along the acoustic focus of the array (Fig. 1). The thin slit diffracts the incoming photoacoustic waves and, hence, improves the receiving aperture along the elevation direction. As shown in Fig. 1, in a conventional linear-array PAT system [Fig. 1(a)], due to elevation focus from the acoustic lens, photoacoustic waves coming out of the focal zone cannot be received by the transducer. The loss in elevation receiving aperture limits the corresponding spatial resolution. The metal slit (with a width close to the 300 μm central acoustic wavelength) eliminates the acoustic focus, still allowing waves coming out of the focal zone to reach the transducer [Fig. 1(b)]. The increased receiving aperture can greatly improve the elevation resolution. Compared to other approaches, our method does not require any modification to scanning geometry; only one elevation scan is needed, as in conventional 3D PAT. This unique feature possesses a significant advantage over existing approaches [9,10].

To validate our assumption, we first imaged a tube filled with black ink. The tube is placed along the lateral direction (y-axis) of the array and can be scanned along the elevation direction (z-axis) through a translation stage. In the z–x plane, the tube looks like a point source [Figs. 1(a) and 1(b)]. Acoustic signals are received by a 128-element linear transducer array (ATL/Philips L7-4) with 5 MHz central frequency and elevation focus at 25 mm. Light illumination was achieved by an Nd:YAG laser (Surelite SL III-10, Continuum) with <10 ns pulses width and 10 Hz pulse repetition frequency (PRF). The output wavelength is 532 nm, and the energy of each pulse is 18 mJ. PA signals received by the L7-4 array were multiplexed and digitalized by a 64-channel ultrasound data acquisition system (Vantage; Verasonics, Inc.; Redmond;

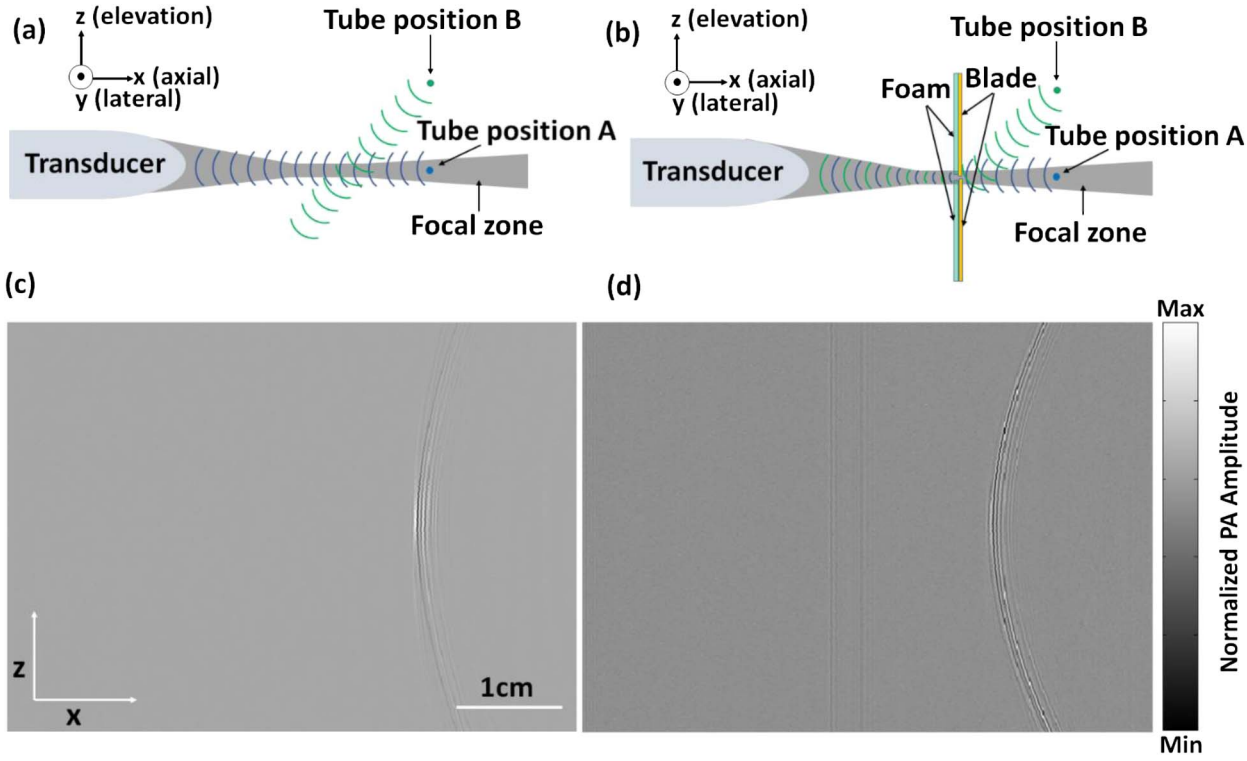

Fig. 1. Principle of slit-enabled PAT. (a) Schematic drawing of conventional PAT and its receiving aperture along the elevation direction. (b) Schematic drawing of slit-enabled PAT and its receiving aperture along the elevation direction. The metal slit is placed between the transducer array and the object. (c) Raw channel data (x–z view) of a tube filled with black ink imaged in conventional PAT. (d) Raw channel data (x–z view) of the same tube imaged in slit-enabled PAT.

Washington). The thin slit was formed by two metal blades (0.5 mm thickness). The bottom blade was fixed in position while the top blade was mounted on a translation stage, which allowed easy and precise control of the slit opening. While our blade thickness is not a multiple of half-acoustic wavelength in stainless steel (0.58 mm), a small portion of sound energy may still transmit directly through the plate [11]. To prevent this, we glued a 5 mm foam on the back surface of the blade (facing the transducer) as an acoustic absorber. As a demonstration of the principle, we scanned over 40 mm with 0.1 mm step size. The entire scan took 80 s (40 mm/0.1 mm/5 Hz).

Figure 1(c) shows a segment of raw-channel data (in z–x plane) acquired without the use of the metal slit. Because of the limited receiving aperture along the elevation direction (the gray-colored region represents the acoustic receiving zone), the transducer gradually misses the tube signal while it is moved from position A to position B. Thus, in Fig. 1(c), only the central region shows a strong tube signal. Once the metal slit has been added [Fig. 1(b)], incoming acoustic waves will diffract through the slit, which changes the wave propagation direction. The tube can now be detected within the entire 40 mm scanning range [Fig. 1(d)]. In principle, the slit can be placed anywhere along the lateral direction. We chose the acoustic focal position because it offers the highest detection sensitivity and minimum signal loss.

Reconstructed images of the single tube are shown in Fig. 2. For the conventional PAT, we used two reconstruction methods. The first method reconstructs each 2D image individually; then all images are stacked to form a 3D image. This is the most commonly used approach to form a 3D image from a linear array [8]. The second method reconstructs the same dataset in 3D using the focal-line concept [12], which improves the elevation resolution up to the size of the elevation focal height (~1.5 mm). Image reconstruction with a slit is similar to the focal-line reconstruction approach [12]. The delay time of each point source in 3D space is calculated based on the following two principles: (1) the wave propagation in x–y plane is unaffected by the slit; and (2) the wave propagation in z–x plane has two segments, first from the point source to the slit and then from the slit to the transducer element. For simplicity, we name the three different reconstruction/imaging methods as 2D-stack PAT, 3D-focal-line PAT, and slit-PAT. As shown in Fig. 2(a) and Visualization 1, 2D-stack PAT has the poorest elevation resolution (along the z-axis). The tube can barely be identified. While 3D-focal-line PAT provides better images of tube structure, the tube image is still blurred along the elevation direction [Fig. 2(b) and Visualization 2]. As expected, slit-PAT offers the highest elevation resolution, and the tube can be clearly identified [Fig. 2(c) and Visualization 3]. It should be noted that, in all these images, we saw two tubes instead of one due to the boundary buildup effect along the axial direction [13]. The distance between the two "tubes" is quantified to be 0.5 mm, which is the inner diameter of the tube.

Table 1 summarizes the elevation resolution and signal-to-noise ratio (SNR) of three imaging/reconstruction methods. The elevation resolution is defined as the full width at half-maximum (FWHM) of the first boundary of the tube along the elevation direction. It can be seen that 2D-stack PAT

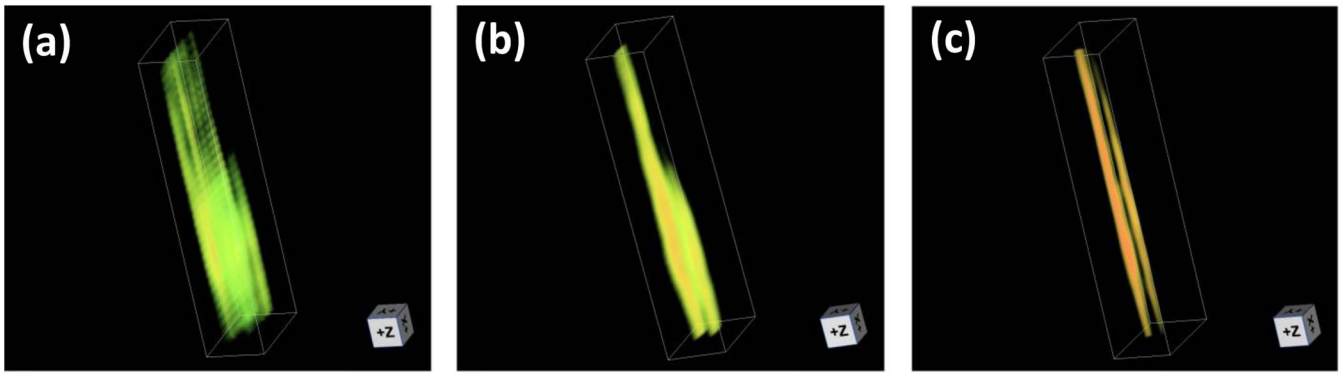

Fig. 2. Reconstructed images of a single tube. (a) 2D-stack PAT image (Visualization 1). (b) 3D-focal-line PAT image (Visualization 2). (c) Slit-PAT image (Visualization 3).

provides the worst elevation resolution. With focal-line reconstruction, the resolution was improved by two times, and the value is close to the height of the elevation focus (1.5 mm). Slit-PAT further improves resolution by almost five times to 0.33 mm, which is close to the 0.3 mm slit opening. In total, slit-PAT offers 10 times better elevation resolution than 2D-stack PAT. Because the slit also blocks some incoming photoacoustic signals, we analyzed the SNR. The signal intensity was calculated by averaging signals within a small region in the tube. Noise was estimated by calculating the standard deviation of signals in a background region. The main source of noise was the electronic noise in the PAT data acquisition system. As shown in Table 1, the slit-PAT SNR is actually four times better than that of 2D-stack PAT. This is due to the fact that, in slit-PAT, the transducer receives signals from all 400 scanning positions, whose data are coherently summed during reconstruction. This procedure reduces the noise by 20 times. In terms of signal intensity, the slit reduces the signal by five times (0.3 mm slit opening/1.5 mm elevation focal height). Thus, the overall improvement in SNR is four times [$\frac{1}{5}$ signal/($\frac{1}{20}$ noise)]. As expected, 3D-focal-line PAT provides the highest SNR. However, due to the limited receiving aperture, its SNR is only two times better than that of slit-PAT, but with five times worse elevation resolution. The resolution and SNR results demonstrate that slit-PAT remarkably improves the elevation resolution without compromising the SNR.

To further demonstrate the imaging capability, we imaged a mouse abdomen *in situ* (Fig. 3). In addition to the hemoglobin contrast, we also used ZnBNc nanonaps as an intestine-confined contrast agent, as previously reported [14]. To match the absorption peak of ZnBNc nanonaps (710 nm), we used light coming out of an optical parametric oscillator (OPO) laser pumped by the Nd:YAG laser. The experiment was performed on a 23 g female nude mouse, which was fasted overnight with access to only water. Before the experiment, the mouse was administered via gavage 0.2 mL of ZnBNc nanonaps with an absorbance of 500 at 710 nm. Thirty minutes after gavage, the mouse was sacrificed and mounted vertically on the system with the abdomen facing the transducer array (Fig. 3). In both the conventional and slit-enabled PAT, we scanned vertically over 25 mm, which covers the entire small intestine region. For better illustration, the reconstructed 3D image was maximum amplitude projected and depth-encoded along the axial direction of the array (posterior direction of the animal body).

Figure 4(a) shows the depth-encoded image of 2D-stack PAT. Anatomical features or structures were not recognizable due to the poor elevation resolution. Figure 4(b) shows a depth-encoded image of 3D-focal-line PAT, where some skin vessels could be recognized. However, body structures were still difficult to recognize. Figure 4(c) shows the depth-encoded image of slit-PAT. Here, we can clearly identify the intestine and several additional skin vessels. In particular, a pair of crossed skin vessels (arrow 2) is only made visible with the high elevation resolution. These features agree well with photos of an exposed animal acquired after the experiment [Fig. 4(d)]. Corresponding 3D images of Figs. 4(a)–4(c) are shown in Visualization 4–Visualization 6, respectively.

In summary, we developed slit-enabled PAT, which significantly improves the elevation resolution of the linear transducer array. For the L7-4 array used in our experiment, the elevation resolution was improved 10 times to 0.33 mm, which is close to the lateral resolution (0.298 mm) and is not far from the axial resolution (0.144 mm). Besides improvement in elevation resolution, the slit also improves the SNR due to a larger receiving aperture. We demonstrated the performance of the system in

Table 1. Elevation Resolution and SNR Analysis of Different Imaging/Reconstruction Methods

	2D-Stack PAT	3D-Focal-Line PAT	Slit-PAT
Resolution	3.52 mm	1.67 mm	0.33 mm
SNR	16.2	136.7	62.7

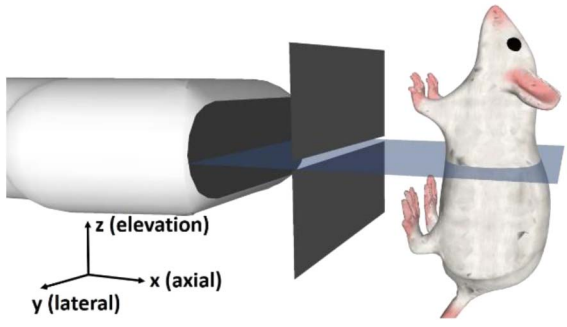

Fig. 3. 3D drawing of the *in situ* experiment setup.

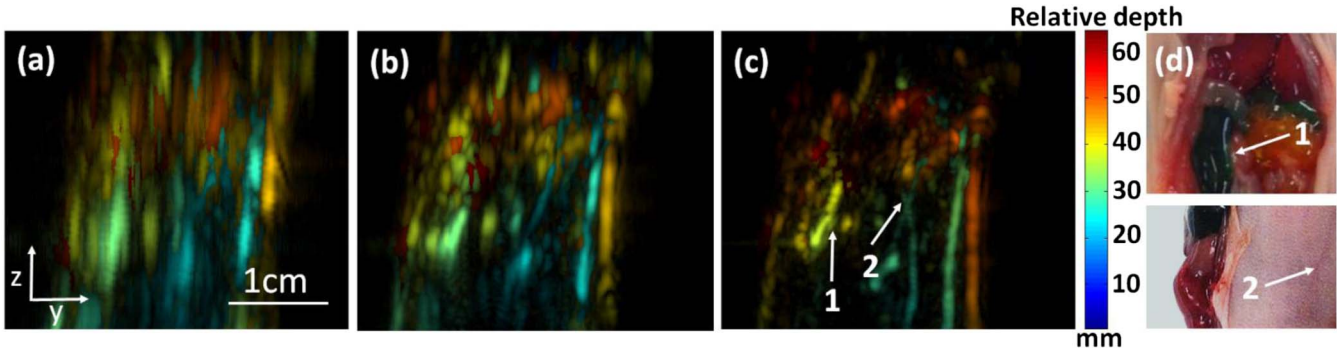

Fig. 4. *In situ* experiment of mouse abdomen. (a) Depth-encoded image of 2D-stack PAT (Visualization 4). (b) Depth-encoded image of 3D-focal-line PAT (Visualization 5). (c) Depth-encoded image of slit-PAT (Visualization 6). Arrows 1 and 2 point to intestine and crossed skin vessels, respectively. (d) Photos of exposed animal, acquired after the PAT experiment. Arrows 1 and 2 point to the same features respectively as in (c). The abdomen and skin were fully intact for (a)–(c).

both phantom and *in situ* and the improvements are obvious. Compared to existing approaches to improve elevation resolution [8,9], our method has the highest imaging speed and requires no change to the scanning geometry. Thus, it can be easily adapted to any existing linear-array PAT systems. Due to limitations in laser pulse repetition rate (10 Hz), we imaged the animal only *in situ* (as animal motion prevents 3D reconstruction). However, kHz high power pulsed lasers are commercially available and can be used for high speed in vivo imaging. In addition, the current setup cannot achieve true isotropic resolution in 3D due to the large element pitch, which defines the lateral resolution. In future studies, we can use a linear phased array or a custom-designed array with smaller pitch to address this issue. Nevertheless, with broad availability of linear arrays, we expect our method to further advance the image quality and application of PAT.

Funding. National Institutes of Health (NIH) (DP5OD017898, R21EY026411); University at Buffalo (UB) (internal funding).

Acknowledgment. This Letter was sponsored in part by University at Buffalo startup funding, the SUNY Brain Network of Excellence Big Idea Award.

REFERENCES

1. J. Xia, J. Yao, and L. V. Wang, Electromagn. Waves **147**, 1 (2014).
2. L. V. Wang and S. Hu, Science **335**, 1458 (2012).
3. J. Xia and L. V. Wang, IEEE Trans. Biomed. Eng. **61**, 1380 (2014).
4. J. Xia, C. Kim, and J. F. Lovell, Curr. Drug Targets **16**, 571 (2015).
5. J. Gateau, M. A. Caballero, A. Dima, and V. Ntziachristos, Med. Phys. **40**, 013302 (2013).
6. G. Li, L. Li, L. Zhu, J. Xia, and L. V. Wang, J. Biomed. Opt. **20**, 066010 (2015).
7. G. Li, J. Xia, L. Li, L. Wang, and L. V. Wang, *SPIE BiOS International Society for Optics and Photonics* (2015), p. 93230I.
8. A. Needles, A. Heinmiller, J. Sun, C. Theodoropoulos, D. Bates, D. Hirson, M. Yin, and F. S. Foster, IEEE Trans. Ultrason. Ferroelectr. Freq. Control **60**, 888 (2013).
9. J. Gateau, M. Gesnik, J.-M. Chassot, and E. Bossy, J. Biomed. Opt. **20**, 056004 (2015).
10. M. Schwarz, A. Buehler, and V. Ntziachristos, J. Biophoton. **8**, 60 (2015).
11. M. Michaud, T. Leong, P. Swiergon, P. Juliano, and K. Knoerzer, Ultrason. Sonochem. **26**, 56 (2015).
12. J. Xia, Z. Guo, K. Maslov, A. Aguirre, Q. Zhu, C. Percival, and L. V. Wang, J. Biomed. Opt. **16**, 090505 (2011).
13. Z. Guo, L. Li, and L. V. Wang, Med. Phys. **36**, 4084 (2009).
14. Y. Zhang, M. Jeon, L. J. Rich, H. Hong, J. Geng, Y. Zhang, S. Shi, T. E. Barnhart, P. Alexandridis, and J. D. Huizinga, Nat. Nanotechnol. **9**, 631 (2014).